Supplemental Data

Heterozygous Deficiency of *PHD2*

Restores Tumor Oxygenation and Inhibits

Metastasis via Endothelial Normalization

Massimiliano Mazzone, Daniela Dettori, Rodrigo Leite de Oliveira, Sonja Loges, Thomas Schmidt, Bart Jonckx, Ya-Min Tian, Anthony A. Lanahan, Patrick Pollard, Carmen Ruiz de Almodovar, Frederik De Smet, Stefan Vinckier, Julián Aragonés, Koen Debackere, Aernout Luttun, Sabine Wyns, Benedicte Jordan, Alberto Pisacane, Bernard Gallez, Maria Grazia Lampugnani, Elisabetta Dejana, Michael Simons, Peter Ratcliffe, Patrick Maxwell, and Peter Carmeliet

SUPPLEMENTAL EXPERIMENTAL PROCEDURES

ANIMALS: C57BL/6 mice (8-12 weeks old) were obtained from our mouse facility. Housing and all experimental animal procedures were approved by the Institutional Animal Care and Research Advisory Committee of the K.U. Leuven.

SYNGENEIC TUMOR MODELS: Two subcutaneous and one orthotopic tumor models were used. IN VIVO SUBCUTANEOUS TUMOR MODELS: B16F10.9 melanoma and Lewis lung carcinoma (LLC) adherent growing murine cells were harvested and single-cell suspensions of $5{\cdot}10^5$ cells in 200 μl (B16) or $1{\cdot}10^5$ cells in 50 μl (LLC) of PBS were injected subcutaneously into the right flank or foot pad of syngeneic mice, respectively. Tumor volumes were measured every two days with a caliper using the formula: $V = \pi \times [d^2 \times D] / 6$, where *d* is the minor tumor axis and *D* is the major tumor axis. The mice were sacrificed at defined time intervals after cell inoculation or when tumors reached a maximum size of 2 cm^3. Growth curves were statistically analyzed using two way-ANOVA. Tumor and lungs were collected for histological analysis. For the LLC model, lung nodules were counted under a stereoscopic microscope. Alternatively the primary tumor was removed by leg amputation when reaching a volume of 800 mm^3 to allow further growth of metastatic nodules; in this model, survival is correlated with pulmonary metastasis (Gao et al., *Science*, **319**, 195-198, 2008). For both models, H&E-stained tumor and lung sections were evaluated by the pathologist for tumor necrosis, invasion and metastasis. IN VIVO ORTHOTOPIC TUMOR MODEL: For orthotopic pancreatic tumor growth, mice were anesthetized with isoflurane, the stomach exteriorized via abdominal midline incision, and 10^6 Panc02 tumor cells in 30 μl PBS were injected into the head of the pancreas using a 29-gauge needle. A successful intrapancreatic injection of tumor cells was identified by the appearance of a fluid bleb without intraperitoneal leakage. Peritoneum and abdominal wall were closed with individual surgical sutures. At day 10, primary tumors were removed, and tumor weight and volume were analyzed as mentioned above. The incidence of tumor invasion into adjacent organs, hemorrhagic ascites, and mesenteric lymph node metastases were recorded. Tumor invasion and necrosis were histologically confirmed as above. All tumor growth experiments were repeated 3 to 8 times, each experiment comprising 6 to 10 mice per group (unless otherwise indicated). Tumor volume and weight shown in the figures and tables are means ± SEM from one representative experiment.

CIRCULATING TUMOR CELLS: $1{\cdot}10^6$ GFP^+ Panc02 tumor cells in 30 μl PBS were injected into the head of the pancreas. At day 12, primary tumors were removed and 1 ml of blood was

collected in heparin. After lysing red blood cells, the cell pellet was washed in PBS and let to adhere on the plastic of a 6 cm- Petri dish. GFP^+ cells were then counted under a fluorescent microscope.

IN VIVO COLONIZATION ASSAY: GFP^+ B16 tumor cells were harvested with EDTA and resuspended in PBS at a final concentration of $4 \cdot 10^5$ cell/ml; 200 μl of cell suspension was injected into the tail vein. After 18 days organs were harvested and weighed. Pulmonary and liver nodules were counted under a stereoscopic microscope.

HISTOLOGY, IMMUNOSTAININGS AND MORPHOMETRIC ANALYSES: All methods for histology and immunostaining have been described (Fischer et al., *Cell*, **131**, 463-475, 2007; Michieli et al., *Cancer Cell*, **6**, 61-73, 2004). For serial sections cut at 8 μm thickness, tissue samples were immediately frozen in OCT compound or fixed in 2% PFA overnight at 4°C, dehydrated and embedded in paraffin. Thick sections (40 μm thickness) were cut after fixing tissue samples in 2% PFA overnight at 4°C, followed by an overnight treatment at 4°C in 30% sucrose solution and frozen in OCT compound. Immunostainings were performed using the following primary antibodies: rat anti-CD31 (BD Pharmingen), rat anti-F4/80/Mac1, rat anti-CD45 (all Becton Dickinson), rabbit anti-fibrin(ogen) (Nordic), mouse anti-α-smooth muscle actin, mouse anti-vimentin, rabbit anti-cytokeratin (Dako), rabbit anti-laminin, rabbit anti-GFP (Molecular Probes), mouse anti-PCNA (Novacastra), rabbit anti-claudin-5, rabbit anti-ZO-1 (Zymed), goat anti-VE-cadherin and goat anti-CD105/endoglin (R&D System), rabbit anti-active caspase 3 (Abcam), rat anti-extracellular Flt1 (Reliatech), rabbit anti-HIF-1α (Novus), rabbit anti-HIF-2α (generated by Patrick Maxwell), and rabbit anti-LYVE-1 (Cell Signalling) and rabbit anti-PHD2 (Lifespan). Sections were then incubated with the appropriate fluorescently conjugated secondary antibodies (Alexa 488 or 546, Molecular Probes) or with peroxidase-labeled IgGs (Dako), followed by amplification with the proper tyramide signal amplification systems when needed (Perkin Elmer, Life Sciences). Morphometric analyses were performed using a Zeiss Axioplan microscope with KS300 image analysis software. Tumor inflammation was analyzed and expressed as the percentage of $CD45^+$ or $F4/80^+$ area over the total tumor area. To assess tumor endothelial cells proliferation, BrdU 200 mg/kg was injected i.p. After 8h tumors were harvested and frozen in OCT compound. Co-immunostainings with rat anti-BrdU (Immunosource) and anti-CD105/endoglin (R&D Systems) were carried out on 4 μm tumor sections. The same tumor sections were analyzed for endothelial apoptosis by coimmunostaining with anti-active caspase-3 and anti-CD105. For all the studies, 5-10 optical fields (20x or 40x magnification) per tumor section were randomly chosen and analyzed by using a Zeiss Axioplan microscope with KS300 image analysis software.

PHYSIOLOGICAL ANGIOGENESIS ASSAYS: Vasculature of yolk sacs was assessed at E9.5 as described (Rolny et al., *Blood*, **108**, 1877-1886, 2006). Embryos at E9.5 and ovaries upon hormone induced-ovulation were processed by overnight fixation in 2% PFA, followed by de-hydration and re-hydration in consecutive series of methanol solutions (25-50-75-100%). After a short wash in PBS, samples were blocked in PBSMT (2% nonfat milk, 0.5% Triton x-100 in PBS). Incubations with both primary and secondary antibodies were done overnight at 4ºC followed by three washes of 1h in PBSMT also at 4°C.

ELECTRON MICROSCOPY: Mice were anesthetized (60 mg/kg Nembutal), perfused with 2% PFA and 2.5% glutaraldehyde in 0.1 M Na-cacodylate buffer, pH 7.2-7.4 for 7 min. Organs were dissected, cross sectioned and fixed overnight in 2% PFA and 2.5% glutaraldehyde in Na-cacodylate buffer. After 24h, 3 rinses of 30 min with 0.1 M Na-cacodylate buffer

were followed by postfixation with 2% osmiumtetroxide in 0.1 M Na-cacodylate buffer for 2h at room temperature. Following dehydration in a graded aceton series (30-50-70-100%) the organs were critical-point dried (Balzers CPD 030). Critical-point dried tissues were mounted on stubs with double-sided adhesive carbon tape. The stubs were coated with gold (SPI-MODULE^{TM} Sputter Coater, SPI Supplies). Images were obtained with a scanning electron microscope (JEOL JSM-6360) at 15 kV (KULeuven, Laboratory of Plant Systematics).

HEMATOLOGICAL ANALYSIS: Blood was collected in heparin with capillary pipettes by retro-orbital bleeding, and white blood cell count determined using a hemocytometer.

CELLS AND CULTURE CONDITIONS: TUMOR CELLS: murine melanoma B16 clone F10.9, and the murine Lewis lung carcinoma (LLC) cell lines were obtained from American Type Culture Collection (ATCC). The murine pancreatic Panc02 tumor cell line was kindly provided by B. Wiedenmann (Charité, Berlin). B16F10.9 and LLC cell lines were maintained in DMEM (Gibco) containing 10% FBS, while the Panc02 cell line was cultured in RPMI (Gibco) containing 10% FBS. All tumor cells were routinely maintained in 5% CO_2 and 95% air at 37°C. For assays in hypoxic conditions, cells were cultured in 2% O_2, 5% CO_2 and 93% N_2. ENDOTHELIAL CELLS (ECS): WT and *PHD2*$^{+/-}$ murine primary endothelial cells were derived from lungs as described (Kuhlencordt et al., *Am J Physiol Cell Physiol*, **5**, 1195-1202, 2004). Briefly, mice were sacrificed by cervical dislocation and lungs were harvested. After a wash in PBS to remove the excess of blood, lungs were minced in RPMI medium containing 0.1% collagenase type I and incubated in the same solution for 1h at 37°C with gently agitation. The digested tissue was passed 10 times by a 19G needle, filtered by a 40 µm pore sized mesh and cells were centrifuged 5 min at 1000 rpm. After red blood cell lysis, the remaining cells were washed in PBS and cultured in DMEM-F12 medium (Gibco) containing 20% FBS, endothelial cells growth factors, heparin and antibiotics in 0.1% gelatin pre-coated plates. When reached confluence, cells were incubated with magnetic beads previously coated with rat anti-ICAM2 (clone 3C4; BD Pharmingen) and endothelial cells were then selected under magnetic field, using a column (MACS; Miltenyi Biotec). Cell purity was then checked by CD31 or CD105 immunostaining. MOUSE EMBRYONIC FIBROBLASTS (MEFS): WT and *PHD2*$^{+/-}$ embryos at day 13.5 were dissected to remove all internal organs. The carcass was minced and the pieces incubated with 0.25% trypsin/EDTA and 10 mg/ml DNase for 30 min at 37°C. Cells were cultured in DMEM medium supplemented with 10% FBS. CANCER-ASSOCIATED FIBROBLASTS (CAFS): WT and *PHD2*$^{+/-}$ CAFs were isolated from GFP^{+} Panc02 tumors. The tumor was rinsed and disaggregated 1h in RPMI 10% FBS with 0.1% collagenase I at 37°C on a rotator. Fibroblasts were sorted (FACSAria; BD Bioscience) by negative selection as CD31^{-}/CD45^{-}/GFP^{-} cells and checked by vimentin staining. TUMOR ENDOTHELIAL CELLS (TECS) were sorted from the same samples by selecting CD31^{+}/CD45^{-}/GFP^{-} cells. LEUKOCYTES were obtained by centrifugation of peripheral blood on a Ficoll gradient. LYMPHATIC ENDOTHELIAL CELLS (LEC) are commercially available from Lonza.

TRANSFECTION OF ENDOTHELIAL CELLS WITH RNAI OLIGOMERS: All RNAi oligomers were designed using the Invitrogen online siRNA design tool (http://rnaidesigner.invitrogen.com). The following sequences (sense strands) and target positions were used: HIF-1α RNAi (position 933): 5'-CCC ATT CCT CAT CCG TCA A-3'; HIF-1α RNAi (position 1832): 5'-GCC TAA CAG TCC CAG TGA A-3'; HIF-2α RNAi (position 566): 5'-GCU UCC UUC GGA CAC AUA A-3'; HIF-2α RNAi (position 1121): 5'-GCC ACA GCA UGG ACA UGA A-3'; control RNAi: 5'-GCC CGA GUA CAG UAA CGA A-

3'. Cells were transfected using Lipofectamine 2000 (Invitrogen) according to the manufacturer's instructions. In brief, one day before transfection, cells were seeded in a 6-well plate in 2 ml of growth medium without antibiotics such that they were 30-50% confluent at the time of transfection. Preparation of the oligonucleotide-Lipofectamine 2000 complexes was done as followed: 100 pmols RNAi oligomers (stock: 20 µM) were diluted in 250 µl Opti-MEM I (Gibco) reduced serum medium. Lipofectamine 2000 (5 µl) was diluted in 250 µl Opti-MEM I and incubated for 5 min at room temperature. RNAi oligomers in Opti-MEM I medium were gently mixed with Lipofectamine 2000 and allowed to incubate at room temperature for 20 min to form complexes. Just before transfection, the cell culture medium was removed and cells were rinsed twice with serum-free Opti-MEM I medium. The Lipofectamine 2000-RNAi complexes were added to each well in serum-free OptiMEM medium for 6h. Afterwards, cells were incubated in complete medium for 48-72h at 37°C and assayed for gene knockdown (qRT-PCR).

IN VITRO BIOLOGICAL ASSAYS: PROLIFERATION ASSAY: $5 \cdot 10^5$ endothelial cells were seeded in gelatin-coated 24-well plate. After 36h of starvation in serum-free medium, subconfluent cell layers were stimulated with 50 ng/ml VEGF (R&D Systems). After 24h, cells were challenged with 10 mM BrdU for 30 min at 37°C. Cells were fixed with 4% PFA and 70% ethanol, then stained with FITC-conjugated anti-BrdU according to the manufacturer's instructions (BD Bioscience). APOPTOSIS ASSAY: subconfluent endothelial cell layers were stimulated in serum-free medium with 50 ng/ml VEGF. After 72h cells were fixed in 4% PFA. TUNEL staining was performed according to manufacturer's instructions (In situ cell death detection kit, Roche). MOTILITY ASSAY: confluent endothelial cell layers seeded on a fibronectin-coated 35 mm tissue culture dish were starved for 48h with 0.5% FBS medium. After scratching the monolayer with a pipette tip, vehicle or VEGF (50 ng/ml) was added in the same growth medium. Images were acquired every 15 min for 6-14h. LAMELLIPODIA AND FILOPODIA FORMATION ASSAY: sparse primary endothelial cells were starved for 48h in 0.5% FBS medium and stimulated with 50 ng/ml VEGF or FGF-2 (R&D Systems) for the indicated times. After fixation, cells were stained with Alexa 488-conjugated phalloidin. Quantification of lamellipodia and filopodia was performed as described (Kitamura et al., *Nat Cell Biol*, **3**, 329-337, 2008; Sheldon et al., *FASEB J*, 2008). TRANS-ENDOTHELIAL ELECTRICAL RESISTANCE (TER) ASSAY: Transwell unit (Costar) were coated with gelatin crosslinked with glutaraldehyde. 50,000 ECs were seeded in the inserts (upper chamber, pore size 0.4 mm) and allowed to reach full confluence in complete medium for 96 hours before measurement. TER was measured using a Multicell-ERS voltohmmeter (Millipore)**.**

ELISA: Concentration of sFlt1 was quantified in endothelial cell medium supernatants using sFlt1 immunoassays (R&D Systems).

IMMUNOPRECIPITATION AND IMMUNOBLOT ANALYSIS: Protein extraction and immunoblot analysis were performed using 1% Triton buffer or 8M urea buffer as described (Michieli et al., *Cancer Cell*, **6**, 61-73, 2004; Sowter et al., *Cancer Res*, **63**, 6130-6134, 2003). Nuclear extraction was performed in cell extracts using a Nuclear and Cytoplasmic Extraction kit (Pierce Biotechnology), according to manufacturer's instructions. Signal was detected using ECL system (Amersham Biosciences) according to the manufacture's instructions. The following antibodies were used: rabbit anti-HIF-2α, rabbit anti-PHD1, rabbit anti-PHD2 (generated by P. Ratcliffe and P. Maxwell), rabbit anti-HIF-1α, rabbit anti-PHD3 (Novus), goat anti-VE-cadherin (R&D Systems), rabbit anti-Flt1 (R&D Systems for the IP and Sigma for the WB), and rabbit anti-ß-tubulin, actin or snRNP (Abcam).

qRT-PCR: Quantitative RT-PCR was performed as described (Fischer et al., *Cell*, **131**, 463-475, 2007), using commercially available or homemade primers and probes for the studied genes. The Assay ID (Applied Biosystems) or the sequence of primers and probes (when home-made) are listed in Table S2.

HYPOXIA ASSESSMENT AND TUMOR PERFUSION: Tumor hypoxia was detected 2h after injection of 60 mg/kg pimonidazole hydrochloride into tumor-bearing mice. Mice were sacrificed and tumors harvested. To detect the formation of pimonidazole adducts, tumor cryosections were immunostained with Hypoxyprobe-1-Mab1 (Hypoxyprobe kit, Chemicon) following the manufacturer's instructions. Tumor perfusion was analyzed using fluorescent microspheres as described (Luttun et al., *Nat Med*, **8**, 831-840, 2002). Perfused tumor vessels were also counted on tumor cryosections by following intravenous injection of 0.05 mg FITC-labelled lectin (*Lycopersicon esculentum*; Vector Laboratories) in tumor-bearing mice. Vessel leakage was analyzed after intravenous injection of 0.25 mg Texas Red-conjugated Dextran 70 kD (Molecular Probes). Ten minutes later, mice were perfused by intracardiac injection of saline (5 min) and 2% PFA (7 min). Tumors were then harvested and frozen in OCT medium. Alternatively, 100 μl of a 3% Evans blue solution were injected into the tail vein and after 10 min mice were perfused, the organs collected in formamide and digested for 24h at 70°C. Concentration of the dye was determined spectrophotometrically at 630 nm.

OXYMETRY, LACTATE AND REDOX POTENTIAL: We measured tumor oxygen tension (pO_2) using charcoal powder (100 mg; CX0670-1; EM Science) as the oxygen-sensitive probe. Calibration curves were made by measuring the EPR line width as a function of the pO_2 (Aragones et al., *Nat Genet*, **2**, 170-180, 2008). Charcoals were injected into 100 mm^3 tumors and oxygen tension was measured after 48h by using an EPR spectrometer (Magnetech) with a low-frequency microwave bridge operating at 1.1 GHz and extended loop resonator. The intratumor levels of lactate were measured as described on snap-frozen tissues, harvested from WT and *PHD2*$^{+/-}$ mice when the tumors were between 200 and 400 mm^3 (Noll, *Methods Enzymatic Analysis*, **6**, 582-588, 1981). NADH and NAD^+ were quantified independently on snap-frozen tumor samples as described (Pospisilik et al., *Cell*, **131**, 476-491, 2007).

STATISTICS: Data represent mean ± SEM of representative experiments unless otherwise stated. Statistical significance was calculated by *t*-test unless otherwise stated (Prism v4.0b), considering $P<0.05$ as statistically significant.

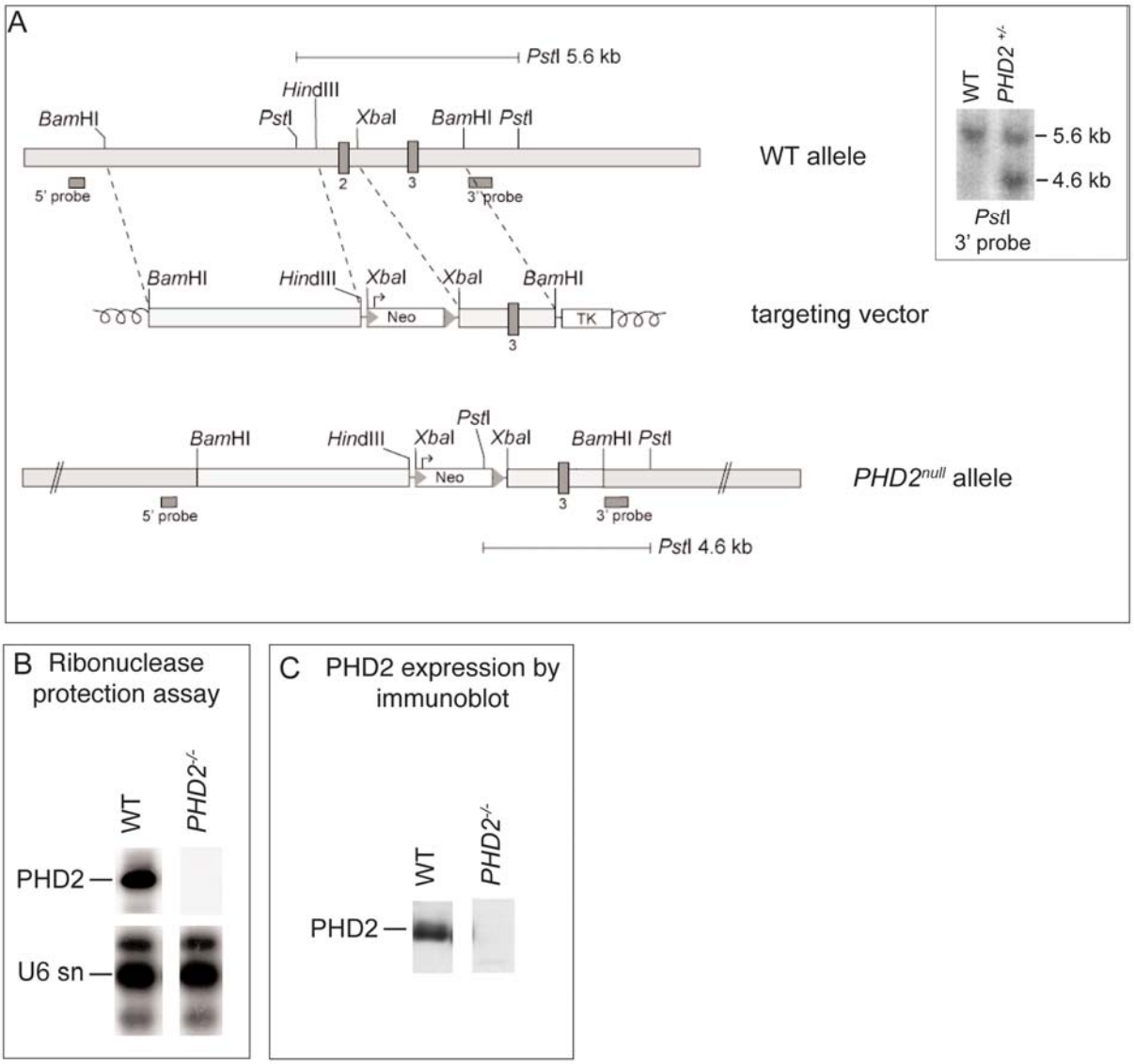

FIGURE S1. GENERATION OF MICE LACKING *PHD2* AND ANALYSIS OF *PHD2* EXPRESSION
A, Targeting strategy for inactivation of the *PHD2* locus. Top: Wild type *PHD2* allele, with relative positions of exons 2 and 3 (dark boxes in genomic structure). Middle: Outline of the targeting vector specifying the genomic sequences used as 5' and 3' homology flanks, cloned at both sides of a neomycine resistance (*Neo*) cassette. A thymidine kinase (*TK*) gene outside the flanking homologies was used for negative selection against random integration events. Bottom: Replacement of exon 2 by the Neo cassette after homologous recombination. A diagnostic restriction fragment generated with *Pst*I is indicated by a thin line under the allele. **Inset:** Southern Blot analysis of genomic DNA from WT and $PHD2^{+/-}$ ES cells, digested with *Pst*I and hybridized with 3' external probe. The 5.6 kb and 4.6 kb fragments correspond to the WT and null *PHD2* allele, respectively. **B,** Ribonuclease protection assay, confirming the absence of PHD2 mRNA transcripts in $PHD2^{-/-}$ embryos. **C,** Immunoblot revealing detectable PHD2 protein in WT but not in $PHD2^{-/-}$ embryos.

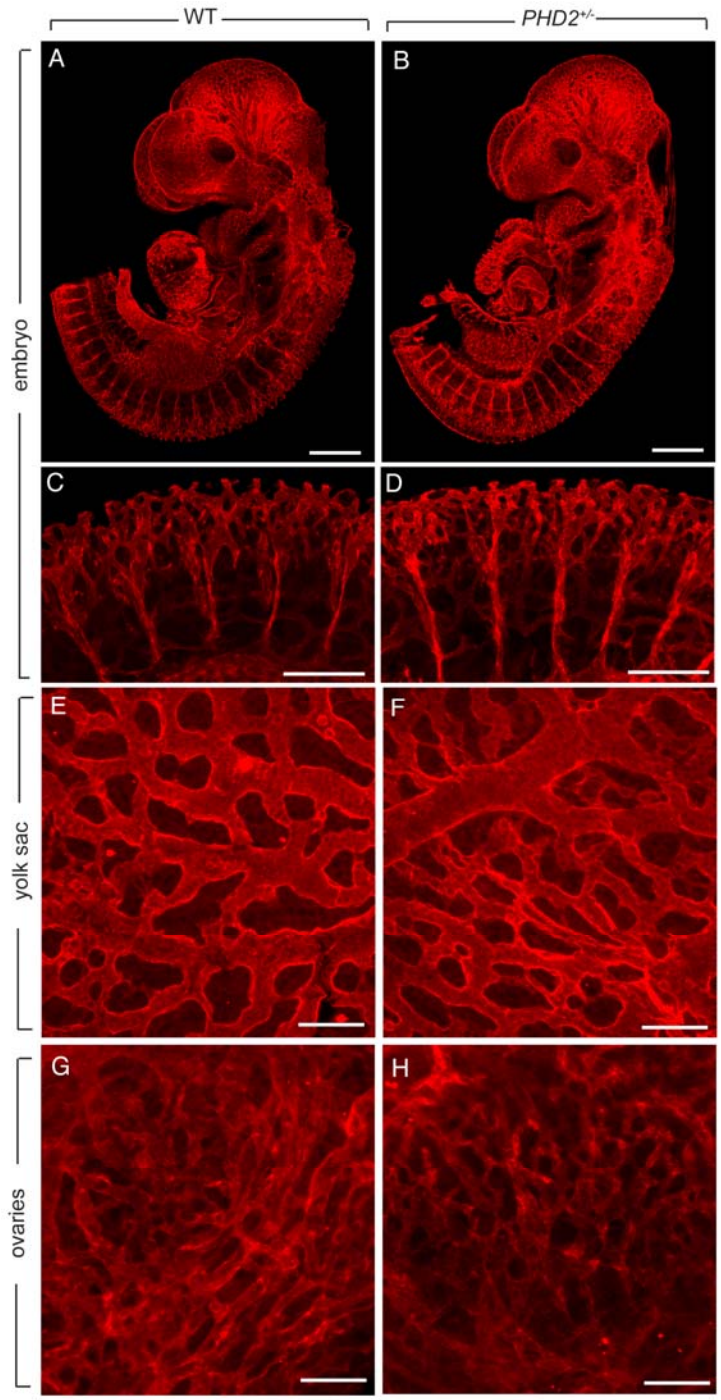

FIGURE S2. NORMAL PHYSIOLOGICAL ANGIOGENESIS IN *PHD2*$^{+/-}$ MICE

A-F, Whole mount immunostaining for the endothelial cell marker CD105, revealing normal vascular development in WT (left) and *PHD2*$^{+/-}$ (right) embryos (E9.5), at a low magnification providing an overview (A,B) and at a high magnification providing a detailed image of the intersomitic vessels (C,D). Panels E,F show normal vascular development in the yolk sac of these *PHD2*$^{+/-}$ embryos. The most caudal part of the embryo was removed for genotyping. **G,H,** Physiological angiogenesis in the ovaries during ovulation is also comparable in both genotypes. Bars: 500 µm in panels A,B; 250 µm in panels C,D; 50 µm in panels E-H.

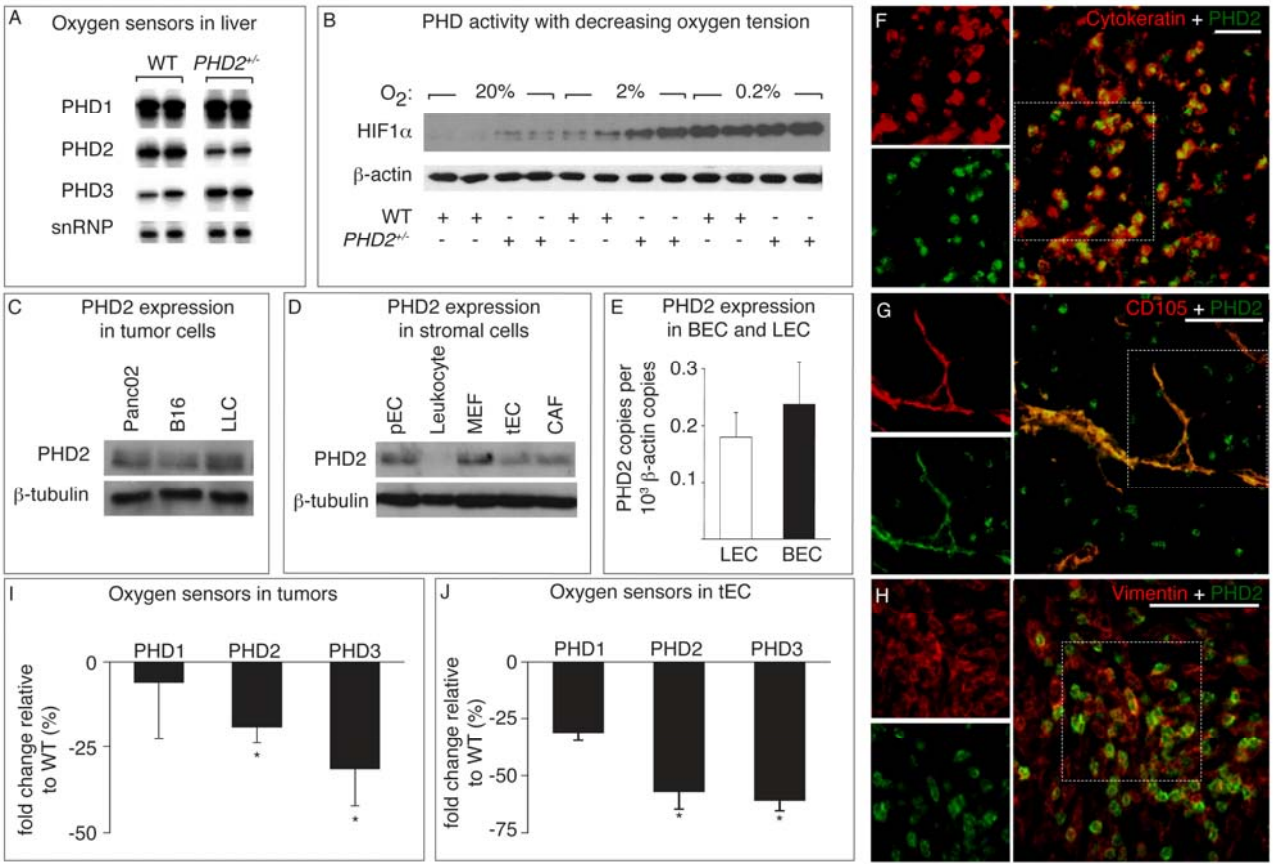

FIGURE S3. EXPRESSION OF PHDS IN NORMAL TISSUES, TUMOR AND STROMAL CELLS

A, Immunoblot for PHDs in WT and *PHD2*$^{+/-}$ livers, revealing ~50% of PHD2 levels and a slight upregulation of PHD3 levels in *PHD2*$^{+/-}$ livers. **B,** Immunoblot for HIF-1α in mouse embryonic fibroblasts (MEF) exposed to various oxygen tensions, revealing an upregulation of HIF-1α levels in hypoxic conditions; HIF-1α levels were higher in *PHD2*$^{+/-}$ cells at every oxygen tension, indicating that PHD2 is still active at low oxygen tensions. **C,D,** Immunoblot for PHD2 in Panc02, B16 and LLC tumor cells (C), endothelial cells (pEC, pulmonary endothelial cells; tEC, tumor endothelial cells), fibroblasts (mouse embryonic fibroblasts, MEF or cancer associated fibroblasts, CAF) and circulating leukocytes (D). **E,** RT-PCR analysis, revealing expression of PHD2 in cultured primary lymphatic endothelial cells (LEC), comparably to blood endothelial cells (BEC). **F-H,** PHD2 coimmunostaining of pancreatic tumor sections in WT mice, revealing PHD2 expression (in green) in cytokeratin^{+} (F) tumor cells, CD105^{+} (G) vessels, vimentin^{+} (H) fibroblasts (all in red). Inset shows a detail in single channel. **I,J,** RT-PCR analysis, indicating that PHD2 and PHD3 transcript levels in pancreatic tumors (I) and tumor endothelial cells freshly isolated from pancreatic tumors without any subculturing (tECs) (J) are reduced in *PHD2*$^{+/-}$ mice; bars represent the downregulation of the indicated genes, as % of the levels in WT mice. Bar: 25 μm in panels F,G,H. Asterisks in panels I,J denote statistical significance ($P<0.05$). Error bars in E,I,J show the standard error of the mean (SEM); all subsequent error bars are defined similarly.

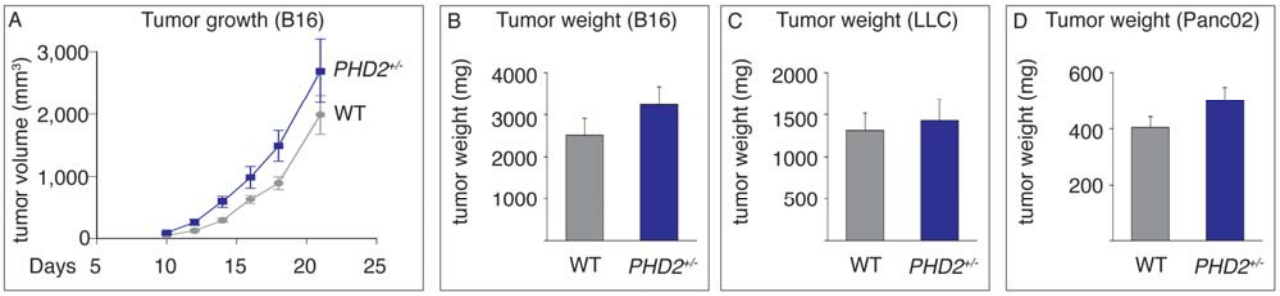

FIGURE S4. NORMAL TUMOR GROWTH IN *PHD2*$^{+/-}$ MICE

A, WT and *PHD2*$^{+/-}$ mice exhibit comparable tumor growth rates after implanting B16 melanoma tumors subcutaneously (N=15; P=0.08). **B-D,** Tumor weight in *PHD2*$^{+/-}$ mice is also comparable for B16 tumors (N=15; P=0.28) (B), LLC tumors (N=8; P=0.33) (C) and pancreatic Panc02 tumors (N=27; P=0.12) (D).

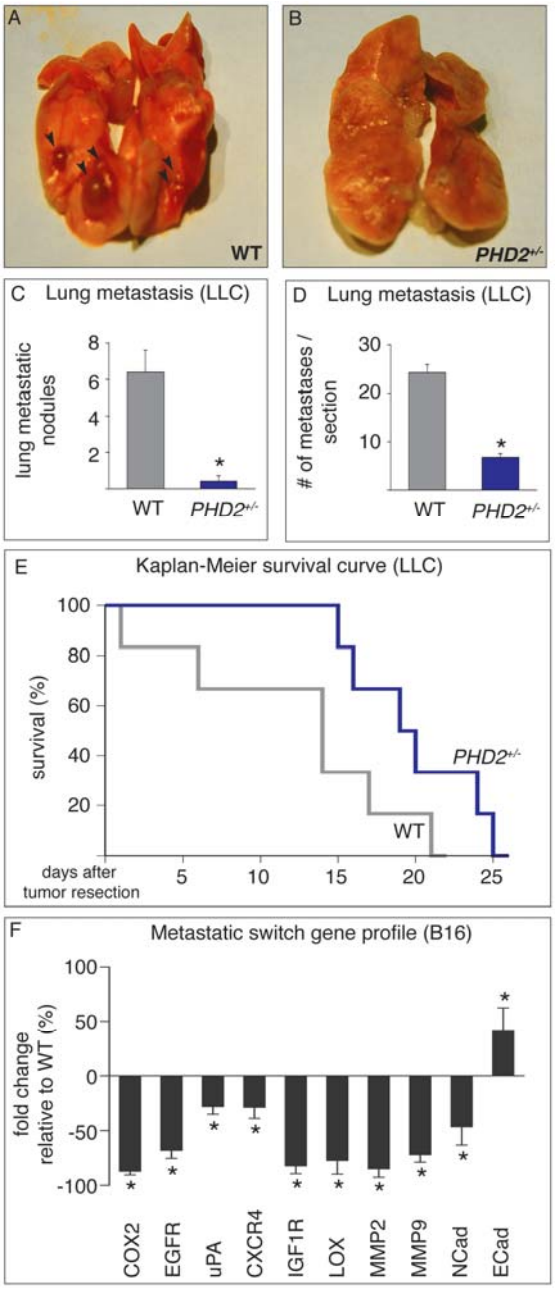

FIGURE S5. REDUCED METASTASIS IN *PHD2*$^{+/-}$ MICE

A,B, Macroscopic view of the lungs, revealing reduced pulmonary metastasis of LLC tumors in *PHD2*$^{+/-}$ mice (arrowheads denote metastatic nodules). **C,D,** Quantification of the number of pulmonary LLC tumor nodules revealed reduced lung metastasis in *PHD2*$^{+/-}$ mice upon macroscopic inspection of the lungs (N=8; P<0.0001) (C), or upon histological analysis of H&E stained sections (N=8; P<0.0001) (D). **E,** Survival curve showing a significant survival benefit of *PHD2*$^{+/-}$ mice; Breslow test (N=6, P=0.04). X-axis indicates days after LLC size-matched tumor resection. **F,** RT-PCR analysis, revealing downregulation of pro-metastatic genes and upregulation of the anti-metastatic E-cadherin gene in B16 tumors in *PHD2*$^{+/-}$ mice; bars represent the upregulation or downregulation of the expression of the indicated genes, expressed as % of the levels in WT mice (N=5-12; P<0.05). Asterisks in panels C,D,E,F denote statistical significance.

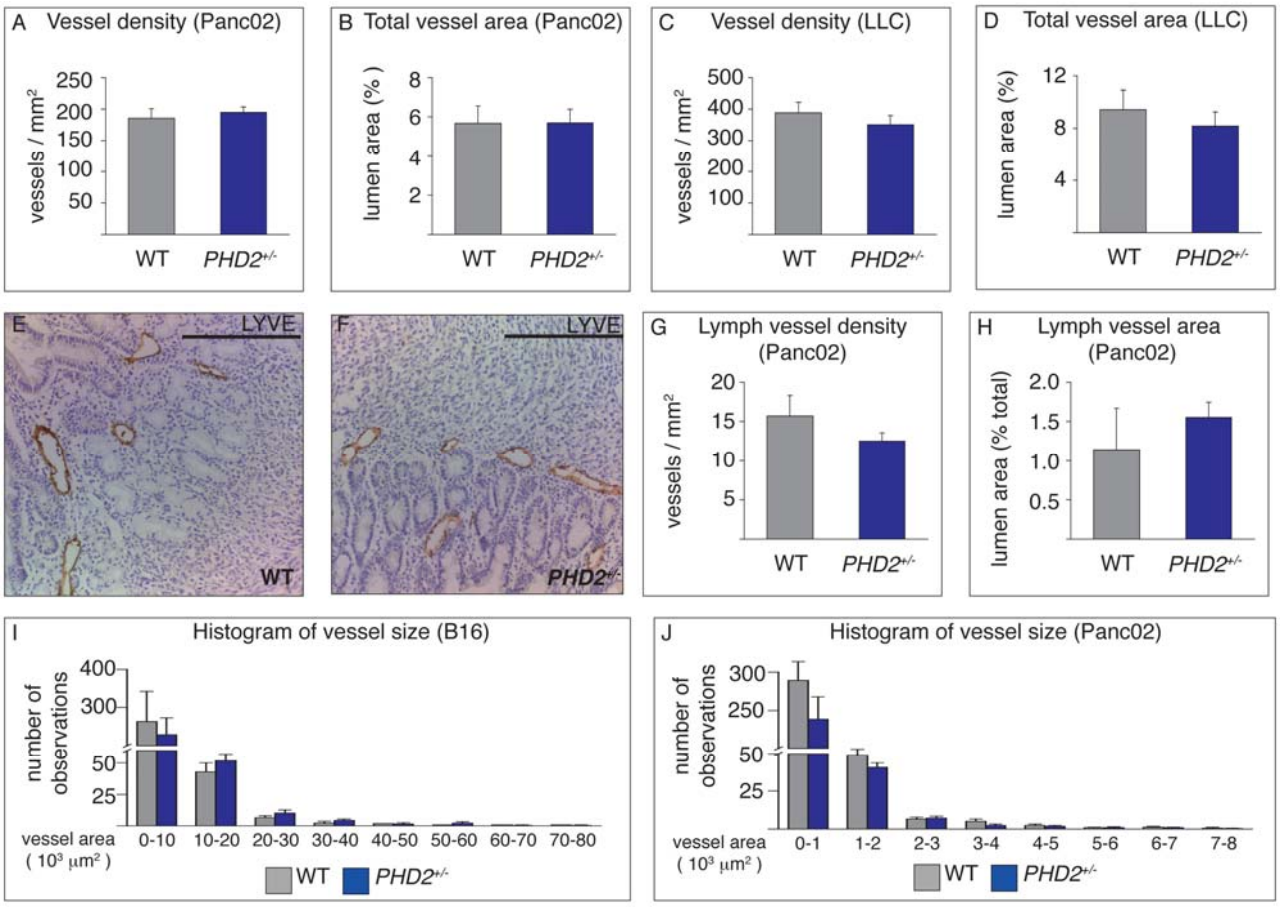

FIGURE S6. TUMOR VESSEL DENSITY, AREA AND DISTRIBUTION IN *PHD2*$^{+/-}$ MICE.
A-D, Morphometric quantification of vessels after CD31 immunostaining in Panc02 (A,B) and LLC (C,D) tumors, revealing comparable vessel density (A,C) and total vessel area (B,D) in tumors in WT and *PHD2*$^{+/-}$ mice (N=6-8; P=NS). **E,F,** Immunostaining for the lymphatic marker LYVE-1, revealing comparable lymphatic density in pancreatic tumors in WT (E) and *PHD2*$^{+/-}$ (F) mice. **G,H,** Morphometric quantification of LYVE-1 stained vessels indicates comparable lymphatic density (G) and lymphatic area (H) in both genotypes. **I,J,** Histogram, revealing a comparable distribution of the number of vessels according to their lumen size in B16 (I) and Panc02 tumors (J) in WT or *PHD2*$^{+/-}$ mice. Bar: 100 µm in panels E,F.

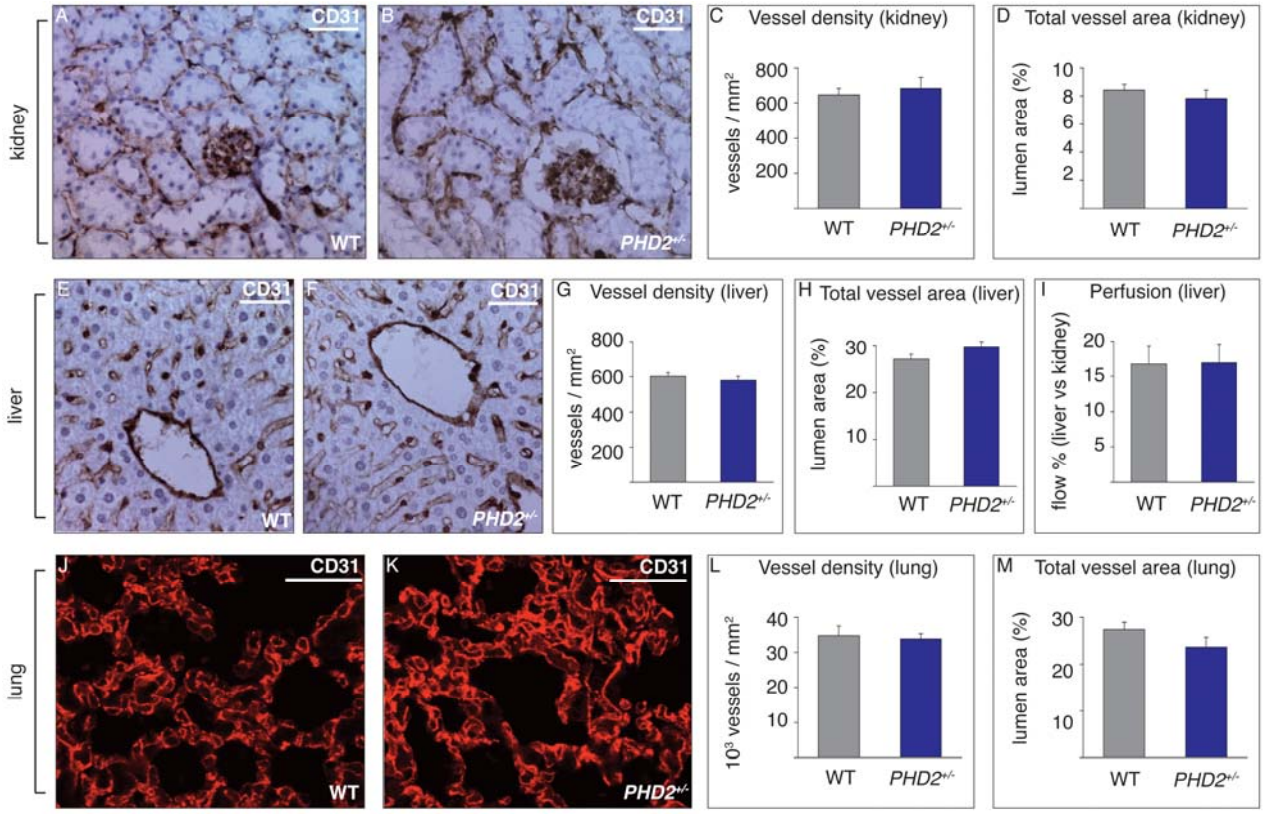

FIGURE S7. VESSEL PHENOTYPE OF HEALTHY ORGANS IN *PHD2*$^{+/-}$ MICE

A,B,E,F,J,K, Immunostaining for CD31, revealing normal vessel development in the kidney (A,B), liver (E,F) and lung (J,K) in WT and *PHD2*$^{+/-}$ mice. CD31 stained cells are brown in panels A,B,E,F and red in panels J,K. **C,D,G,H,L,M,** Quantification of vessel parameters revealed comparable vessel density and total vessel area in the kidney (C,D), liver (G,H) and lung (L,M) in WT and *PHD2*$^{+/-}$ mice (N=4; P=NS). **I**, Liver perfusion, analyzed by the injection of fluorescent microspheres, is comparable in both genotypes. Bar: 100 µm in panels A,B,E,F,J,K.

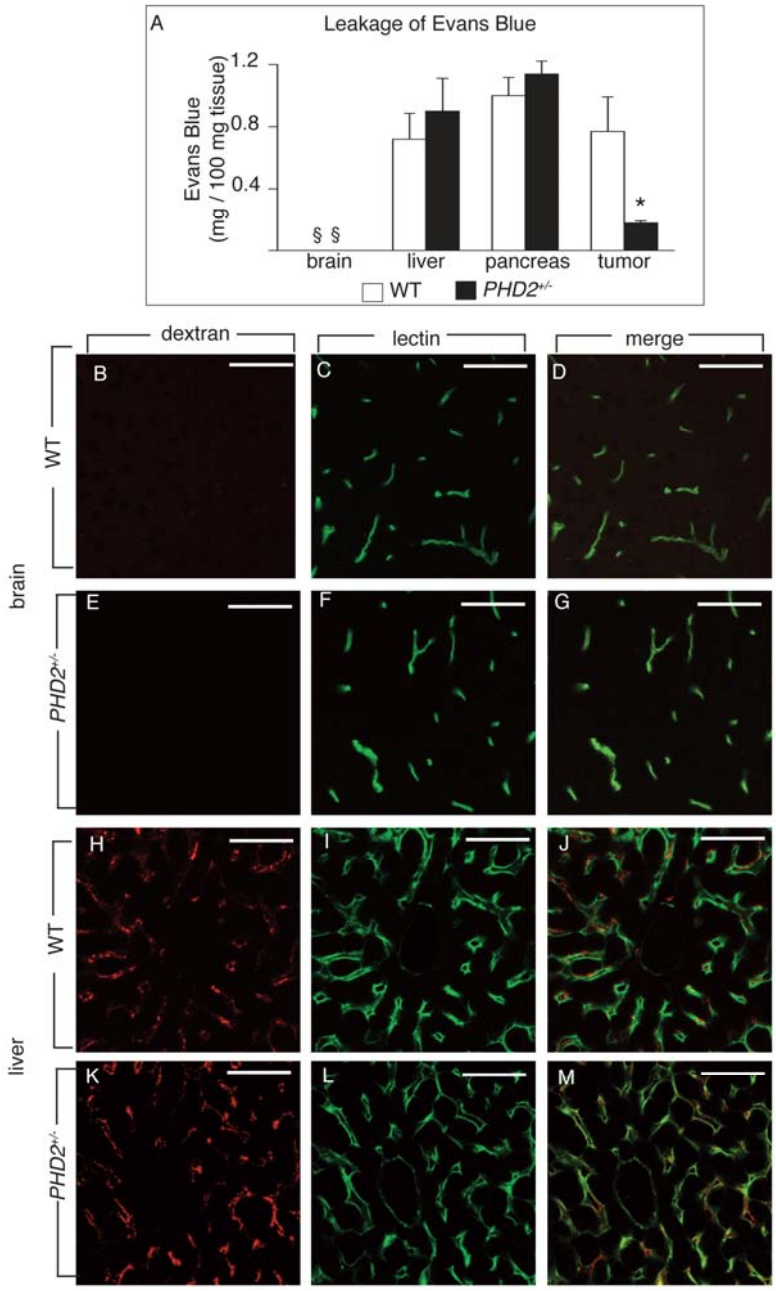

FIGURE S8. VESSEL PERMEABILITY IN *PHD2*$^{+/-}$ MICE

A, Quantification of the amount of extravasated Evans blue, revealing that permeability is high in hepatic and pancreatic vessels and minimal in brain vessels, but comparable in WT and *PHD2*$^{+/-}$ mice. By contrast, leakiness of tumor vessels was significantly reduced in *PHD2*$^{+/-}$ mice (N=5; P=0.03). § denotes below detection limit. **B-M,** Healthy non-tumor-bearing WT and *PHD2*$^{+/-}$ mice were injected with Texas Red-conjugated dextran and FITC-conjugated lectin. After 10 minutes, mice were saline perfused and organs were harvested for fixation; hence, dextran is only visible at sites of vessel leakage. Detection of dextran (red) and lectin (green) on cryosections reveals leakage of dextran through discontinuous liver sinusoidal endothelia (H-M), but not through tightly connected endothelial cells of the blood-brain barrier (B-G) in both genotypes, indicating that permeability of healthy vessels was comparable in WT and *PHD2*$^{+/-}$ mice. Bar: 25 μm in panels B-M. Asterisk in panel A denotes statistical significance.

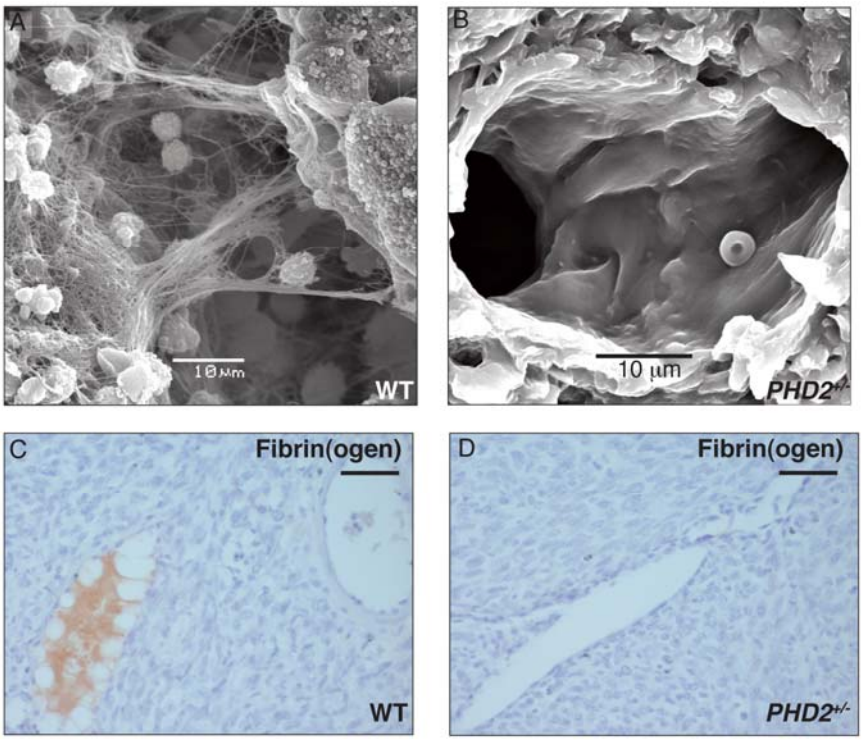

FIGURE S9. REDUCED INTRATUMURAL CLOTTING IN *PHD2*$^{+/-}$ MICE

A,B, Scanning electron microscopy, revealing the presence of intravascular fibrin threads in tumor vessels of a Panc02 tumor in a WT (A) but not in a *PHD2*$^{+/-}$ mouse (B). **C,D,** Immunostaining for fibrin(ogen), indicating less intratumoral clotting in a *PHD2*$^{+/-}$ (D) compared to WT mice (C) (N=6; P=0.01). Bar: 50 µm in panels C,D.

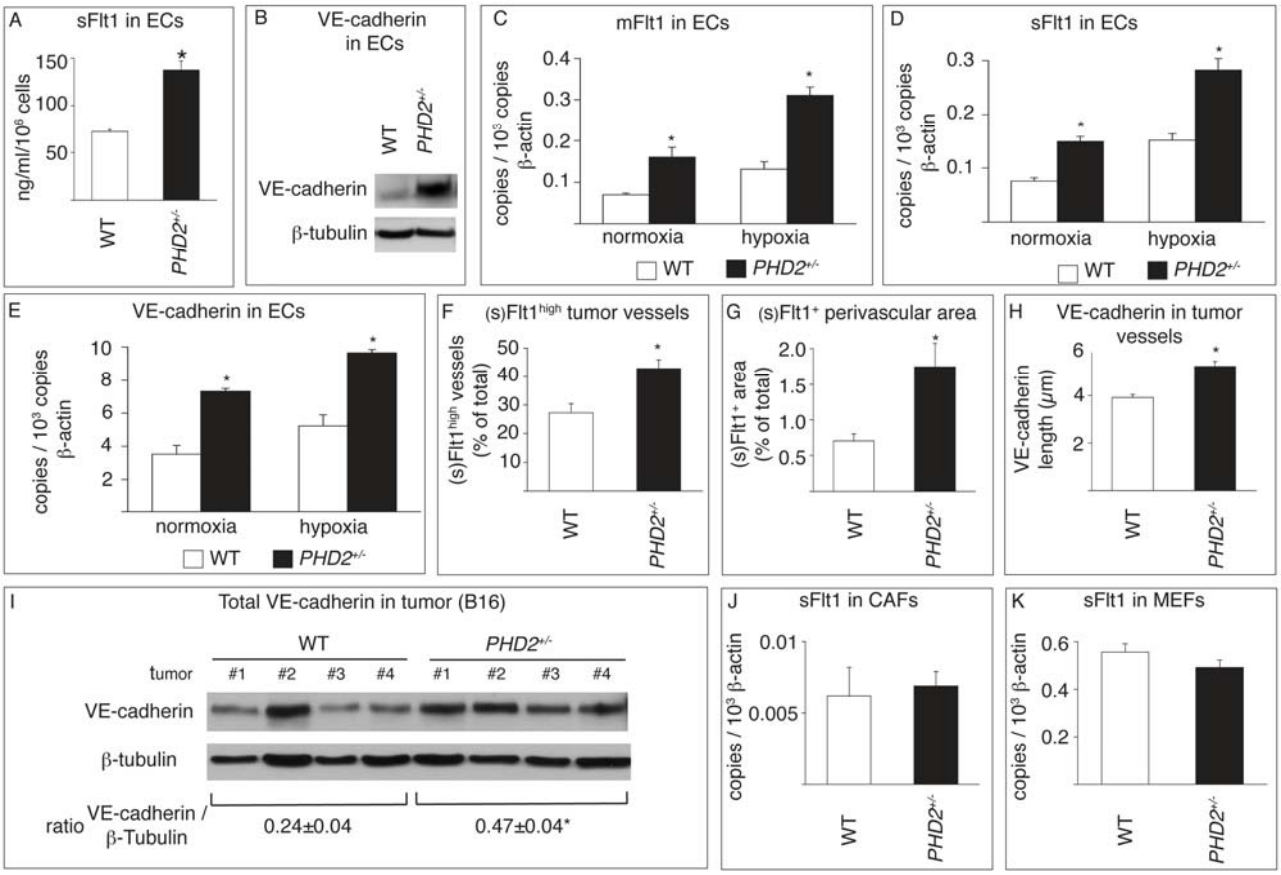

FIGURE S10. ENHANCED SFLT1 AND VE-CADHERIN LEVELS IN *PHD2*$^{+/-}$ ENDOTHELIAL CELLS
A, ELISA revealing increased levels of sFlt1 in conditioned medium of primary *PHD2*$^{+/-}$ lung endothelial cells. **B,** Immunoblot revealing increased levels of VE-cadherin in *PHD2*$^{+/-}$ endothelial cells. **C-E,** RT-PCR analysis, revealing increased mRNA levels of membrane bound Flt1 (mFlt1) (C), sFlt1 (D) and VE-cadherin (E) in *PHD2*$^{+/-}$ endothelial cells in normoxia and hypoxia (1% oxygen). **F,G,** Morphometric quantification of tumor sections immunostained for the endothelial marker CD105 and (s)Flt1 (using an antibody that recognizes the extracellular portion of Flt1) revealing that the number of (s)Flt1^{+} tumor vessels (F) and the accumulation of sFlt1 in the vascular and perivascular tumor environment (G) are increased in *PHD2*$^{+/-}$ mice. **H,** Morphometric quantification of tumor sections immunostained for the endothelial marker CD105 and VE-cadherin revealing that tumor endothelial cells in *PHD2*$^{+/-}$ mice expressed longer VE-cadherin^{+} junctions. **I,** Immunoblot revealing increased VE-cadherin levels in B16 tumors in *PHD2*$^{+/-}$ mice (by densitometric quantification, 2-fold increase in [VEC/ß-tubulin] ratio) (N=4, P=0.006). **J,K,** RT-PCR analysis, revealing comparable sFlt1 transcript levels in *PHD2*$^{+/-}$ cancer-associated fibroblasts (CAFs) or mouse embryonic fibroblasts (MEFs). Asterisks in panels A,C,D,E,F,G,H,I denote statistical significance (P<0.05).

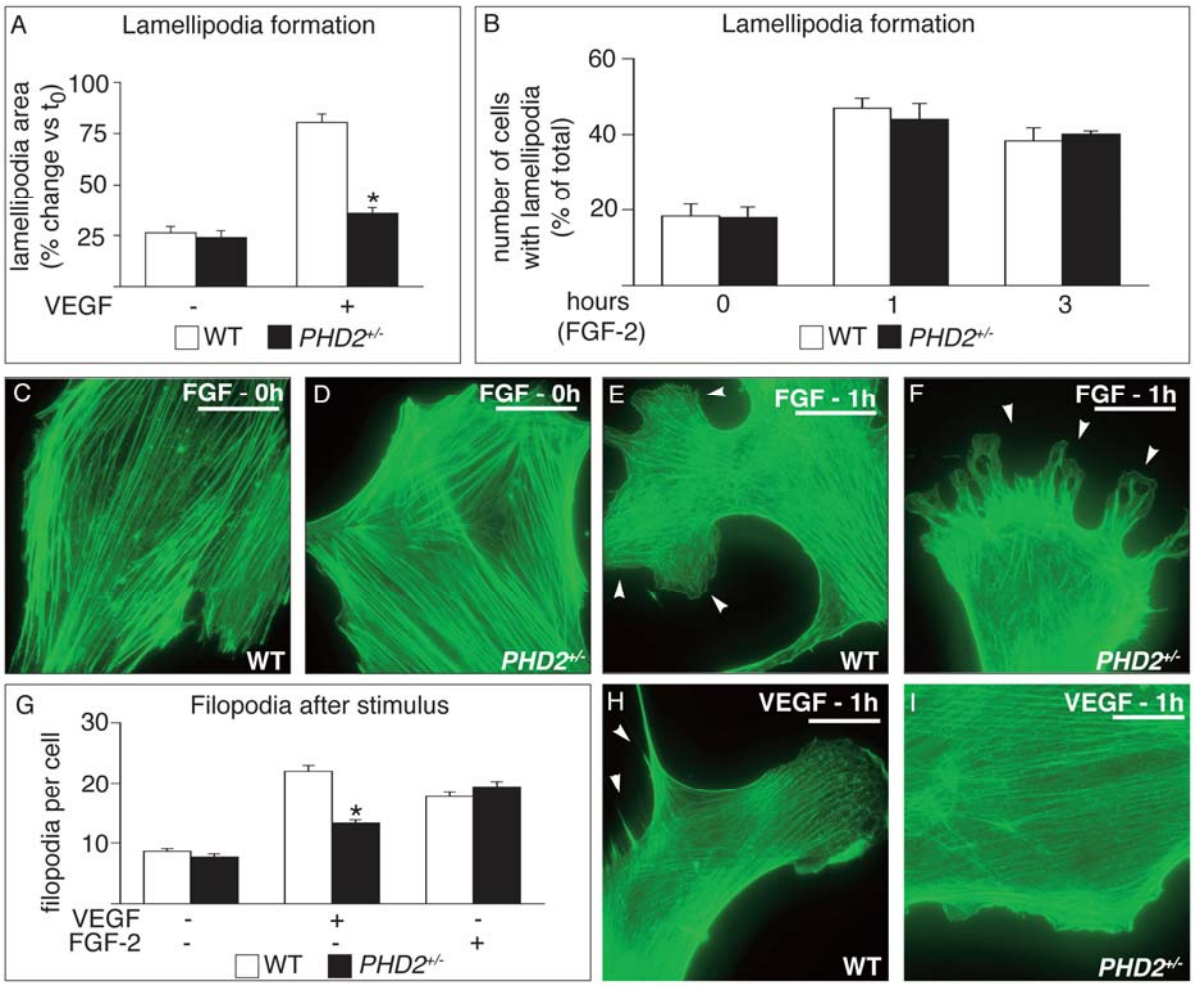

FIGURE S11. IN VITRO CHARACTERIZATION OF *PHD2*$^{+/-}$ ENDOTHELIAL CELLS

A,B, Reduced lamellipodia formation of *PHD2*$^{+/-}$ endothelial cells in response to VEGF. Panel A shows the reduction of lamellipodial area in *PHD2*$^{+/-}$ endothelial cells upon VEGF stimulation; the data are expressed as % of change after 1 hour of stimulation *versus* the start of the experiment (t_0). Panel B shows the % of endothelial cells displaying lamellipodia upon 1 and 3 hours FGF-2 stimulation. **C-F,** Phalloidin staining, revealing a comparable distribution of actin filaments in a WT (C) and *PHD2*$^{+/-}$ (D) endothelial cell in baseline conditions. In addition, reorganization of the actin cytoskeletal network and lamellipodia formation (arrowheads) are comparable in WT (E) and *PHD2*$^{+/-}$ (F) endothelial cells upon stimulation with FGF-2. **G-I,** Reduced filopodia formation of *PHD2*$^{+/-}$ endothelial cells in response to VEGF but not FGF-2. Panel G shows the measurement of the number of filopodia per cell at the start of the experiment (t_0) and after 1 hour of simulation with VEGF or FGF-2, in WT and *PHD2*$^{+/-}$ endothelial cells. Phalloidin staining in panel H,I indicates reduced filopodia formation in a *PHD2*$^{+/-}$ endothelial cell upon VEGF stimulation (I) as compared to a WT cell (H) (arrowheads indicate filopodia). Bar: 50 μm in panels C,D,E,F,H,I. Asterisks in panels A,G denote statistical significance ($P<0.05$).

TABLE S1. HEMATOLOGICAL PARAMETERS OF *PHD2*$^{+/-}$ MICE

	FEMALES		MALES	
	WT	***PHD2*$^{+/-}$**	**WT**	***PHD2*$^{+/-}$**
WBC (K/µl)	4.8 ± 0.6	5.1 ± 0.6	4.3 ± 0.6	4.2 ± 0.6
RBC (M/µl)	7.0 ± 0.1	7.5 ± 0.1*	7.4 ± 0.1	7.8 ± 0.1 *
HGB (g/dl)	11.5 ± 0.2	12.5 ± 0.1*	11.8 ± 0.2	12.8 ± 0.2*
HCT (%)	51.1 ± 1.1	55.9 ± 0.5 *	54.7 ± 0.9	59.3 ± 1.7*
MCHC (G/dl)	22.2 ± 0.4	22.3 ± 0.1	21.6 ± 0.3	21.7 ± 0.3
PLT (K/µl)	195 ± 56	181 ± 55	337 ± 99	338 ± 121

The data represent hematological parameters (mean ± SEM) in WT and *PHD2*$^{+/-}$ mice grouped by gender (N=16-19 per group). Abbreviations: white blood cell (WBC), red blood cell count (RBC), hemoglobin (HGB), hematocrit (HCT), mean cell hemoglobin concentration (MCHC), and platelet count (PLT). * P<0.05.

TABLE S2. LIST OF PRIMERS, USED FOR RT-PCR

GENE	PROBE	FORWARD	REVERSE
ANG-1	AAG-CAA-CAA-CTG-GAC-CTC-ATG-GAC-ACA-GT	CAA-CAA-CAA-CG-CAT-CCT-GCA	TGC-AAA-GGC-TGA-CAA-GGT-TAT-G
COX2	TCA-TGA-GCA-GTC-CCC-TCC-CTA-GGA-CTT-AA	TTT-CAT-CTG-AAG-ACG-GTC-CTC-CA	GGC-CTG-GGA-TGG-CAT-CA
EGFR	AGC-AAC-AAT-TCC-ACT-GTG-GCT-TGC-ATT	CCT-CCT-GAG-TTC-TCT-GAG-TGC-AAC	CAC-GGC-AGC-TCC-CAT-TTC-TA
ENOS	ACT-ATA-ACT-CCA-TCA-AAA-GGA-GTG-GCT-CCC-AG	AGC-CCG-GGA-CTT-CAT-CAA-TC	TGA-AGC-CGC-TGC-TCA-TGA-G
N-CADHERIN	TCT-GTA-TGC-CGC-ATT-CCA-GGC-CG	GGA-CGT-CAT-TGT-AGC-CAA-CCT-AA	CCT-GTA-GGG-TCT-CCA-CCA-CTG-A
PDGF-B	CCC-ATC-TTC-AAG-AAG-	CGG-TCC-AGG-TGA-	CGT-CTT-GGC-TCG-

	GCC-ACA-GTG-ACC-T	GAA-AGA-TTG	CTG-CTC
PFK	ACC-CGT-GGC-TCT-CGT-CTC-AAC-ATC-A	GCC-GGC-TCA-GTG-AGA-CAA-G	TGG-CAC-CTT-TCA-GCA-ACA-ATG
PHD2	ACG-AAA-GCC-ATG-GTT-GCT-TGT-TAC-CCA	GCT-GGG-CAA-CTA-CAG-GAT-AAA-C	CAT-AGC-CTG-TTC-GTT-GCC-T
ROBO4	CAC-GAC-TGC-CAG-GCT-CCT-ATT-GTG-TG	ACA-GAC-CCA-GCT-GGA-GAT-CG	TCC-AGT-GAC-TGC-AGC-CAC-TT
SFLT1	TTT-GCC-GCA-GTG-CTC-ACC-TCT-AAC-G	GAA-GAC-ATC-CTT-CGG-AAG-CAC-GAA	TTG-GAG-ATC-CGA-GAG-AAA-ATG-G
TIE-2	TGC-CTC-CTA-AGC-TAA-CAA-TCT-CCC-AGA-GCA-ATA	AAC-CAA-CAG-TGA-TGT-CTG-GTC-CTA-T	GCA-CGT-CAT-GCC-GCA-GTA
UNC5B	CCA-TTC-CCC-AGG-GCA-AGT-TCT-ATG-ACC	AGC-CTG-TTG-GTA-CCA-AAT-GGA	TTT-CGG-CCT-TGT-TGA-TAT-GTA-GAT-AC
UPA	TGC-TGT-CTA-GAG-CCC-AGC-GGC-A	CCG-CTG-CAG-TCA-CCG-AA	GCC-AGC-CAG-ACT-TTC-ATG-GT
VEGFR-3	CGG-CGA-GCC-CCA-CTT-GTC-CA	GGT-TCC-TGA-TGG-GCA-AAG-G	TCA-GTG-GGC-TCA-GCC-ATA-GG

For the following genes with sequence ID (enclosed between brackets), commercially available primers were ordered from Applied Biosystems (https://products.appliedbiosystems.com): *alpha-5* (MM00434506_m1), *alpha-V* (MM00439797_m1), *angiomotin* (MM00462731_m1), *ß-actin* (MM00607939-s1), *CXCR4* (MM01292123_m1), *Dll4* (MM00444619_m1), *E-cadherin* (MM00486906_m1), *FOXO-1* (MM00490672_m1), *GLUT-1* (MM00441473_m1), *Hes-1* (MM00468601_m1), *Hey-1* (MM00468865_m1), *Hey-2* (MM00469280_m1), *HGFR* (MM00434924_m1), *IGF1R* (MM00802831_m1), *Jagged-1* (MM00496902_m1), *LOX* (MM00495386_m1), *MMP2* (MM00439506_m1), *MMP9* (MM00442991_m1), *Notch-1* (MM00435245_m1), *Notch-2* (MM00803077_m1), *Notch-4* (MM00440510_m1), *Npn-1* (MM01253210_m1), *Nrarp* (MM00482529_m1), *PDK1* (MM00554306_m1), *PDK4* (MM00443325_m1), *PlGF* (MM00435613_m1), *Rgs5* (MM00501393_m1), *Sirt-1* (MM00490758_m1), *TSP-1* (MM01335418_m1), *VE-cadherin* (MM00486938_M1), *VEGF-A* (MM00437306_m1), *VEGF-B* (MM00442102_m1), *mFlt1* (MM01210866_m1) and *VEGFR-2* (MM01222419_m1).

SUPPLEMENTAL REFERENCES

Aragones, J., Schneider, M., Van Geyte, K., Fraisl, P., Dresselaers, T., Mazzone, M., Dirkx, R., Zacchigna, S., Lemieux, H., Jeoung, N.H.*, et al.* (2008). Deficiency or inhibition of oxygen sensor Phd1 induces hypoxia tolerance by reprogramming basal metabolism. Nat Genet *40*, 170-180.

Chan, D.A., Sutphin, P.D., Yen, S.E., and Giaccia, A.J. (2005). Coordinate regulation of the oxygen-dependent degradation domains of hypoxia-inducible factor 1 alpha. Molecular and cellular biology *25*, 6415-6426.

Epstein, A.C., Gleadle, J.M., McNeill, L.A., Hewitson, K.S., O'Rourke, J., Mole, D.R., Mukherji, M., Metzen, E., Wilson, M.I., Dhanda, A.*, et al.* (2001). C. elegans EGL-9 and mammalian homologs define a family of dioxygenases that regulate HIF by prolyl hydroxylation. Cell *107*, 43-54.

Fischer, C., Jonckx, B., Mazzone, M., Zacchigna, S., Loges, S., Pattarini, L., Chorianopoulos, E., Liesenborghs, L., Koch, M., De Mol, M.*, et al.* (2007). Anti-PlGF inhibits growth of VEGF(R)-inhibitor-resistant tumors without affecting healthy vessels. Cell *131*, 463-475.

Gao, D., Nolan, D.J., Mellick, A.S., Bambino, K., McDonnell, K., and Mittal, V. (2008). Endothelial progenitor cells control the angiogenic switch in mouse lung metastasis. Science *319*, 195-198.

Kitamura, T., Asai, N., Enomoto, A., Maeda, K., Kato, T., Ishida, M., Jiang, P., Watanabe, T., Usukura, J., Kondo, T.*, et al.* (2008). Regulation of VEGF-mediated angiogenesis by the Akt/PKB substrate Girdin. Nat Cell Biol *10*, 329-337.

Kuhlencordt, P.J., Rosel, E., Gerszten, R.E., Morales-Ruiz, M., Dombkowski, D., Atkinson, W.J., Han, F., Preffer, F., Rosenzweig, A., Sessa, W.C.*, et al.* (2004). Role of endothelial nitric oxide synthase in endothelial activation: insights from eNOS knockout endothelial cells. Am J Physiol Cell Physiol *286*, C1195-1202.

Luttun, A., Tjwa, M., Moons, L., Wu, Y., Angelillo-Scherrer, A., Liao, F., Nagy, J.A., Hooper, A., Priller, J., De Klerck, B.*, et al.* (2002). Revascularization of ischemic tissues by PlGF treatment, and inhibition of tumor angiogenesis, arthritis and atherosclerosis by anti-Flt1. Nature medicine *8*, 831-840.

Michieli, P., Mazzone, M., Basilico, C., Cavassa, S., Sottile, A., Naldini, L., and Comoglio, P.M. (2004). Targeting the tumor and its microenvironment by a dual-function decoy Met receptor. Cancer cell *6*, 61-73.

Noll, F. (1981). L-(+)-Lactate. Methods of enzymatic analysis *6*, 582-588.

Pan, Y., Mansfield, K.D., Bertozzi, C.C., Rudenko, V., Chan, D.A., Giaccia, A.J., and Simon, M.C. (2007). Multiple factors affecting cellular redox status and energy metabolism modulate hypoxia-inducible factor prolyl hydroxylase activity in vivo and in vitro. Molecular and cellular biology *27*, 912-925.

Pospisilik, J.A., Knauf, C., Joza, N., Benit, P., Orthofer, M., Cani, P.D., Ebersberger, I., Nakashima, T., Sarao, R., Neely, G.*, et al.* (2007). Targeted deletion of AIF decreases mitochondrial oxidative phosphorylation and protects from obesity and diabetes. Cell *131*, 476-491.

Rolny, C., Nilsson, I., Magnusson, P., Armulik, A., Jakobsson, L., Wentzel, P., Lindblom, P., Norlin, J., Betsholtz, C., Heuchel, R.*, et al.* (2006). Platelet-derived growth factor receptor-beta promotes early endothelial cell differentiation. Blood *108*, 1877-1886.

Sheldon, H., Andre, M., Legg, J.A., Heal, P., Herbert, J.M., Sainson, R., Sharma, A.S., Kitajewski, J.K., Heath, V.L., and Bicknell, R. (2008). Active involvement of Robo1 and Robo4 in filopodia formation and endothelial cell motility mediated via WASP and other actin nucleation-promoting factors. Faseb J.

Sowter, H.M., Raval, R.R., Moore, J.W., Ratcliffe, P.J., and Harris, A.L. (2003). Predominant role of hypoxia-inducible transcription factor (Hif)-1alpha versus Hif-2alpha in regulation of the transcriptional response to hypoxia. Cancer research *63*, 6130-6134.

Stolze, I.P., Tian, Y.M., Appelhoff, R.J., Turley, H., Wykoff, C.C., Gleadle, J.M., and Ratcliffe, P.J. (2004). Genetic analysis of the role of the asparaginyl hydroxylase factor inhibiting hypoxia-inducible factor (HIF) in regulating HIF transcriptional target genes. The Journal of biological chemistry *279*, 42719-42725.